

COVER SHEET

Paper Number: **101**

Title: **Fuselage versus Subcomponent Panel Response Correlation Based on ABAQUS Explicit Progressive Damage Analysis Tools**

Authors: Kevin E. Gould
Arunkumar Satyanarayana
Philip B. Bogert

ABSTRACT

Analysis performed in this study substantiates the need for high fidelity vehicle level progressive damage analyses (PDA) structural models for use in the verification and validation of proposed sub-scale structural models and to support required full-scale vehicle level testing. PDA results are presented that capture and correlate the responses of sub-scale 3-stringer and 7-stringer panel models and an idealized 8-ft diameter fuselage model, which provides a vehicle level environment for the 7-stringer sub-scale panel model. Two unique skin-stringer attachment assumptions are considered and correlated in the models analyzed: the TIE constraint interface versus the cohesive element (COH3D8) interface. Evaluating different interfaces allows for assessing a range of predicted damage modes, including delamination and crack propagation responses. Damage models considered in this study are the ABAQUS built-in Hashin procedure and the Complete STress Reduction (COSTR) damage procedure implemented through a VUMAT user subroutine using the ABAQUS/Explicit code.

Keywords: *Damage Model, Progressive Damage Analysis, Tied Interface, Cohesively Bonded, Delamination, 3-Stringer Panel, 7-Stringer Panel, Fuselage*

Kevin E. Gould, Analytical Mechanics Associates, Inc., 21 Enterprise Pkwy, Suite 300, Hampton, VA 23666-6413, U.S.A.

Arunkumar Satyanarayana, NASA Langley Research Center, Mail Stop 431, Hampton, VA 23681, U.S.A.

Philip B. Bogert, NASA Langley Research Center, Mail Stop 190, Hampton, VA 23681, U.S.A.

INTRODUCTION

Composite materials are being widely used in aerospace applications; however, the performance capabilities of composites remain a work in progress due to the immaturity of the tools used to model and predict the behavior of such material, the limited usage of this material option in the aerospace industry, and the limited data available from physical design experiments of varying geometry and scale. Nevertheless, aerospace engineers, and those of other industries, are being challenged to design, test, and qualify composite components faster and cheaper. One of the current objectives of the Advanced Composites Project (ACP) at NASA Langley Research Center (LaRC) is to reduce the time it takes to certify future aircraft constructed from composite materials [1]. While it is important to improve analysis tools at all levels, scaling up tools that are useful at the vehicle level is one avenue that could lead to future designs that are lighter due to a reduction in conservatism resulting from an understanding of failure modes at the structural level.

Additionally, as ACP seeks to improve preliminary rapid design tools, a high fidelity tool at the structural level is useful to provide a comparison for the results obtained from rapid design tools for problems involving large 2-bay cracks.

In order to improve efficiency of the progressive damage analysis (PDA) methods used previously [2,3,4,5] in simulating damage modes for flat notched panels loaded uniaxially, the authors have been adopting a number of new features. These features have been integrated with the current PDA methods making the features more suitable for large curved stiffened structure under combined mechanical and internal pressure loading. These features include, but are not limited to: cohesively bonded elements between stringers and curved skins to simulate delamination and alternatively curved tied interfaces; load introduction structure for more realistic flight loads such as fuselage bending moments; time step and mass scaling to minimize kinetic energy in simulating static response with an explicit dynamic approach; through-the-thickness bending of shell structure; and appropriately varied mesh densities used to conduct PDA simulations.

The ABAQUS/Explicit code, version 6.13-3, was used exclusively to generate the predictions presented in this paper. The ABAQUS built-in damage model, using the Hashin failure criteria with a corresponding failed element deletion scheme, and the Complete STress Reduction (COSTR) damage model [3], which employs the Hashin Rotem failure criteria were utilized for the damage simulation predictions. The composite material selected for the analytical models is consistent with the properties of T800 fiber and an epoxy resin [4]. All components of the finite element models (FEM) possess the same quasi-isotropic stacking sequence [45/90/-45/0]_s. Analysis was performed for both tensile and compressive loading, with pressure, on a structure with a severed stringer and skin to form a central circumferential notch.

In addition to simulating fuselage structure response with complex loading, the authors took advantage of the opportunity to compare the results obtained from sub-component notched panels at the 3-stringer and 7-stringer levels, with test appropriate boundary conditions, to better understand the sub-component size required to simulate the conditions in a full fuselage barrel. Analysis predictions

for all cases will be summarized to include key observations related to: far-field strain comparisons at damage initiation and failure onset; failure load predictions for tied versus bonded interface simulations, and failure load predictions for a typical axially loaded 3-stringer panel, a 7-stringer panel and a “idealized” fuselage structure of 8-ft diameter subjected to specific aircraft maneuver loads.

3-STRINGER MODEL DISCRIPTION

A curved 3-stringer panel 80 inches in length, with a 20.6-inch arc length, stringer spacing of 6.85 inches, and four frames at 20-inch spacing with mouse holes allowing continuous stringer attachment, was used at the outset to conduct a series of sub-component analyses (i.e., uniaxial tension and compression) from which performance was rated. A circumferential notch, which spans 6.85 inches, was formed by detaching the nodes in both the skin and stringer, and is centrally located on the panel. The FEM of the structure is modeled using S4R shell elements. The geometry of the panel stringers and frames are presented in Figures 1(a) and 1(b), respectively. The inner mold line (IML) view of the panel and the relative variation in the mesh density is presented in Figure 2. In the model, the coupling of the skin and stringer contact surfaces is varied to represent three unique cases, which are referred to herein as: (1) “TIED”, (2) cohesive contact, and (3) COH3D8 elements. Note, the foam core of the hat stiffeners is not represented in either of the models.

For the model that contains the discrete adhesive (COH3D8 element) layers, the areas where adhesive exists are depicted in Figure 3(a). The COH3D8 elements are attached to the mating component surfaces via a TIE constraint. The cohesive zone modeling parameters are obtained based on guidance published in Albert Turon’s paper, Reference [6]. Nominal shell element edge length in the refined mesh region is 0.12 inch. The nominal edge length of the COH3D8 elements is 0.04 inch, and the element thickness is specified in the analysis input as zero, as is the case for a bonded panel. The difference in the mesh densities of the shell and COH3D8 element meshes is shown in Figure 3(b).

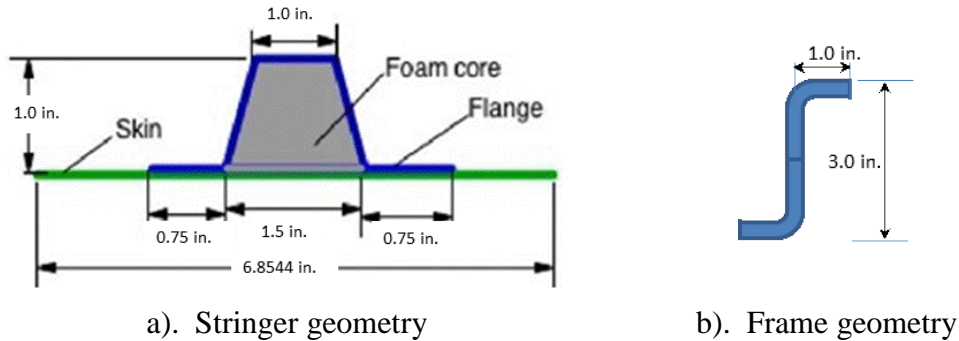


Figure 1. Panel stringer and frame details.

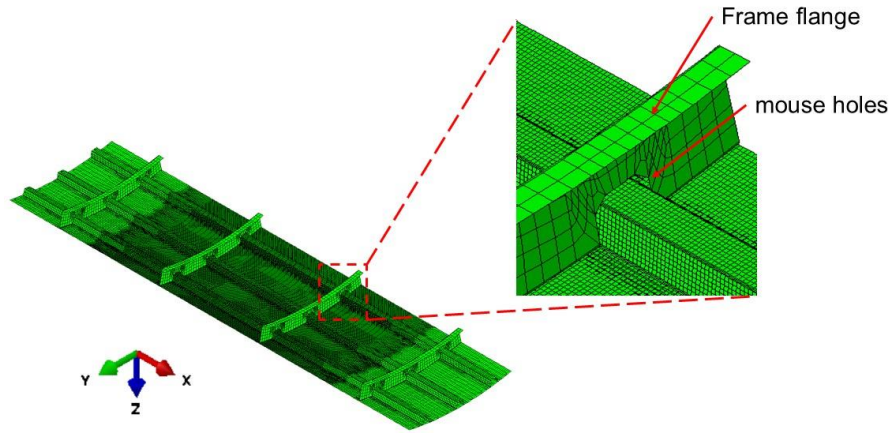
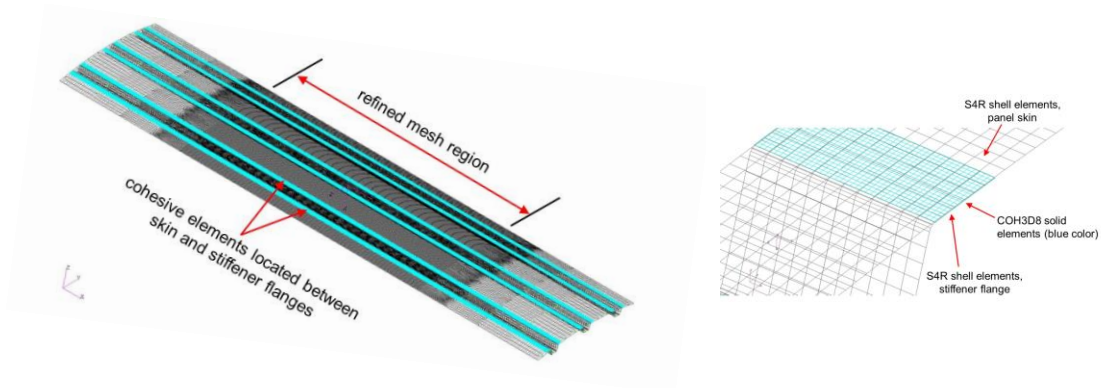


Figure 2. 3-stringer panel configuration – IML View.



a). Cohesive element layers (COH3D8)

b). COH3D8 element layer

Figure 3. Discrete adhesive element layer (COH3D8) modeling.

The fixed mass scaling scheme was applied in all ABAQUS built-in damage model analysis cases to obtain an average speed-up for computation time by a factor of 7.5 over the un-scaled analysis.

3-STRINGER PANEL ANALYSIS AND EVALUATION

Simulations were performed using the 3-stringer model described in the previous section with the three unique skin-stringer interfaces. The objective was to determine which models provided relatively reasonable response predictions when subjected to uniaxial mechanical load, internal pressure, and boundary conditions associated with test stands commonly used at LaRC. The ABAQUS/Explicit code, version 6.13-3, and its built-in Hashin damage model was

used for all 3-stringer panel predictions. The 3-stringer model was used during this investigative phase so that multiple analysis cases could be run concurrently, results obtained quickly, and post-processed in a relatively short timeframe. The boundary conditions used for analyzing the 3-stringer model are depicted in Figure 4. The response obtained for uniaxial tension load only is presented in Figure 5. Small black dots denote the predicted failure load points. The stiffness and final displacement predictions of the cohesive contact model did not correlate well with the responses produced by the other models. The predicted delamination results from uniaxial tension loading of the cohesive contact and the COH3D8 element models are presented in Figures 6(a) and 6(b), respectively. The models capable of capturing delamination were rated against each other to determine which model was best suited for delamination predictions on a larger scale. Based on the results presented in Figure 6, and other factors not discussed herein, a judgment was made to use just two of the three models going forward: the model containing the TIED interface and the model with the COH3D8 element interface. The model with the cohesive contact interface did not correlate well with the other models in all cases considered and was deficient in capturing the delamination failure mode. Only limited delamination is captured in Figure 6(a) over the first adjacent stringer even beyond the panel failure load.

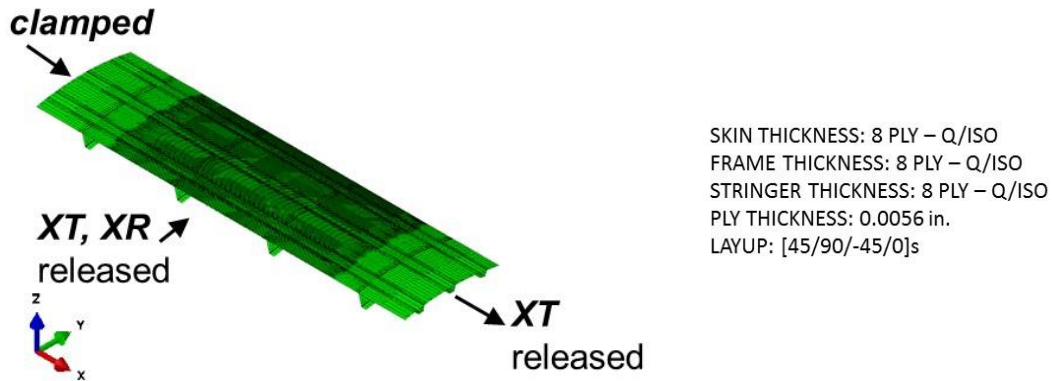


Figure 4. 3-stringer FEM boundary conditions.

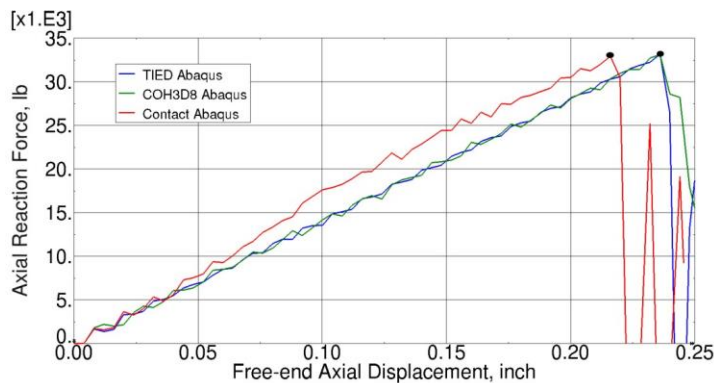
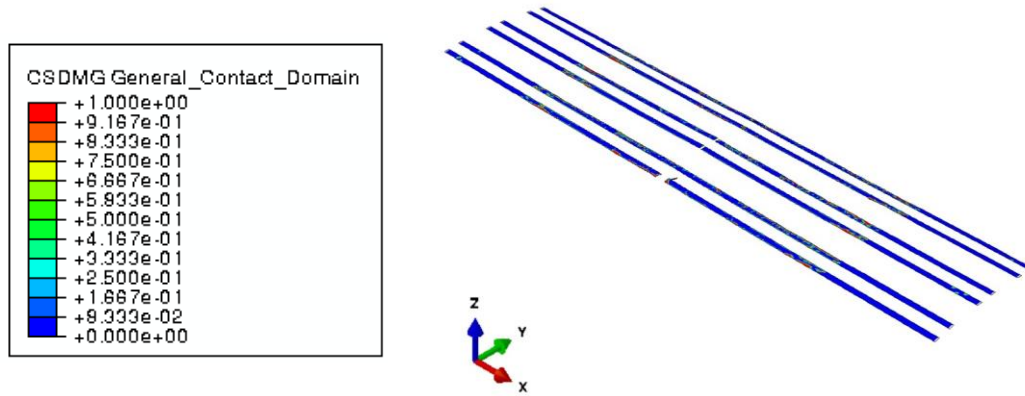
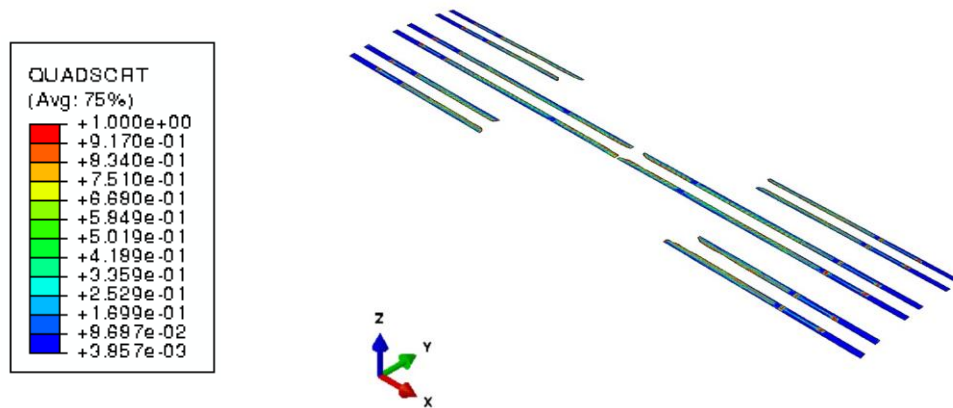


Figure 5. 3-stringer uniaxial tension versus axial displacement predictions.



a). Cohesive Contact Model



b). COH3D8 Element Model

Figure 6. 3-stringer model delamination predictions post final failure.

7-STRINGER PANEL AND IDEALIZED FUSELAGE MODEL DISCRIPTION

Results presented for the 7-stringer FEM correspond to the model shown in Figure 7. The 7-stringer panel FEM, which is essentially the parent model of the 3-stringer panel FEM, was initially created for investigative purposes. However, the 7-stringer model was deemed too expensive computationally for investigative use. The largest elements in the model, which are located along the sides of the panel, are 0.5 inch in the axial direction by 0.96 inch in the circumferential direction. The smallest elements, which make up the central refined uniform mesh region, have an edge length of 0.12 inch. In Figure 7, the dark shaded longitudinal strips, which are imposed in the image are the COH3D8 element layers which are incorporated into the model to capture delamination. Also, the relative variation in the mesh density of the skin of the panel is depicted.

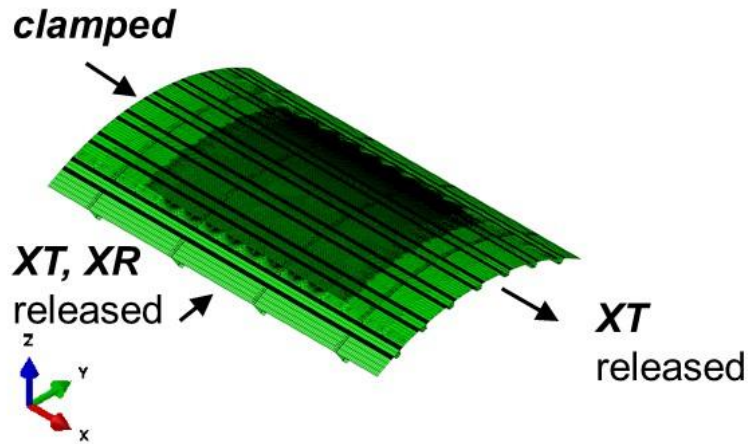


Figure 7. 7-stringer model FEM boundary conditions.

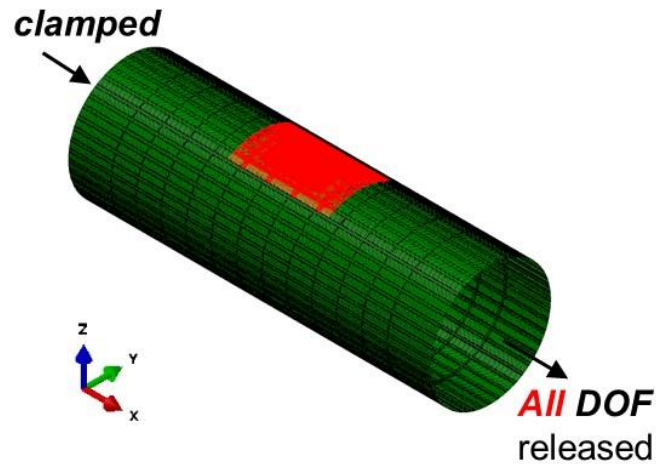


Figure 8. Idealized fuselage FEM boundary conditions.

The idealized fuselage FEM shown in Figure 8, also referred to as “the barrel”, contains the 7-stringer panel FEM embedded in the crown, with a surrounding uniform mesh with elements the same size as those noted above at the sides of the 7-stringer panel FEM. Note, however, that the mesh density of the stringers located in the keel of the barrel, at mid-span, is also refined. The barrel has a length of 288 inches (24-ft), a diameter of 96 inches (8-ft), contains 12 frames at 20-inch spacing, and 44 stringers with the same stringer spacing as noted for the 7-stringer panel. The stringers and frames are attached via the TIE constraint away from the detailed 7-stringer section, highlighted red in Figure 8.

7-STRINGER PANEL PDA PREDICTIONS

The TIED and COH3D8 ABAQUS FEMs and the COH3D8 COSTR FEM were analyzed under combined pressure with axial tension, and pressure with axial compression load cases. Both ABAQUS damage models results shown in Figure 9, captured a load drop at the approximate load of 83 kips, which represents the predicted failure load for the TIED ABAQUS model. The COH3D8 ABAQUS model continues to carry load, albeit with extensive crack growth, and yields a predicted failure load of 104 kips. A by-product of delamination in some cases is load redistribution and additional load resistance [5]. The COSTR model predicted the highest failure load of 109.4 kips. The predicted crack paths for all three models were self-similar, and are presented in Figures 10(a), 10(b), and 10(c). The progression of the crack path over the refined region of the panel occurs quickly in the ABAQUS models and more gradually in the COSTR damage model. Also, the COSTR model predicts delamination to occur prior to ultimate failure of the panel. The predicted delamination progression of the COSTR model, with increasing load, is presented in Figures 11(a), 11(b), and 11(c). The red portions of the cohesive regions shown are fully debonded areas.

The axial compression reaction loads of all the models shown in Figure 12 track closely right up until the predicted failures of the COH3D8 ABAQUS and COSTR models at around 70 kips. The TIED surfaces model, as expected, predicts a higher axial compression failure load of approximately 93 kips. This result holds true because, in compression, the cohesive bond is more vulnerable, reducing its load carrying capacity. The predicted crack path and damage near the notch region of each model are captured at their respective predicted failure loads and have been exploded for visual clarity and are shown in Figures 13(a), 13(b), and 13(c).

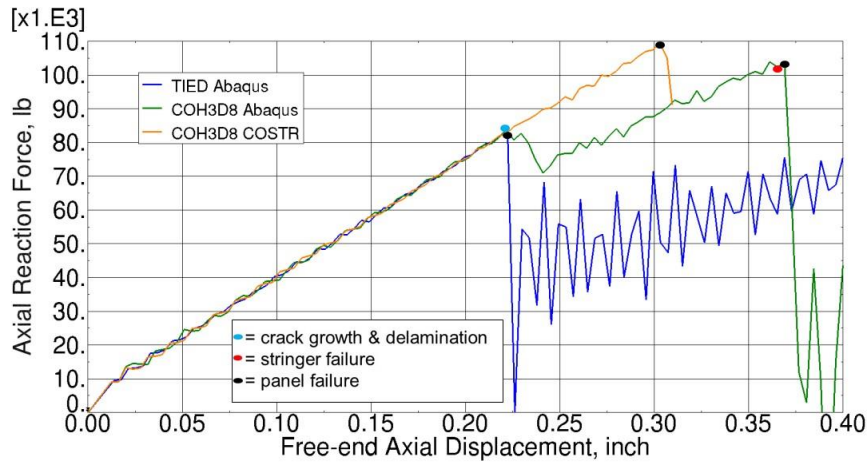
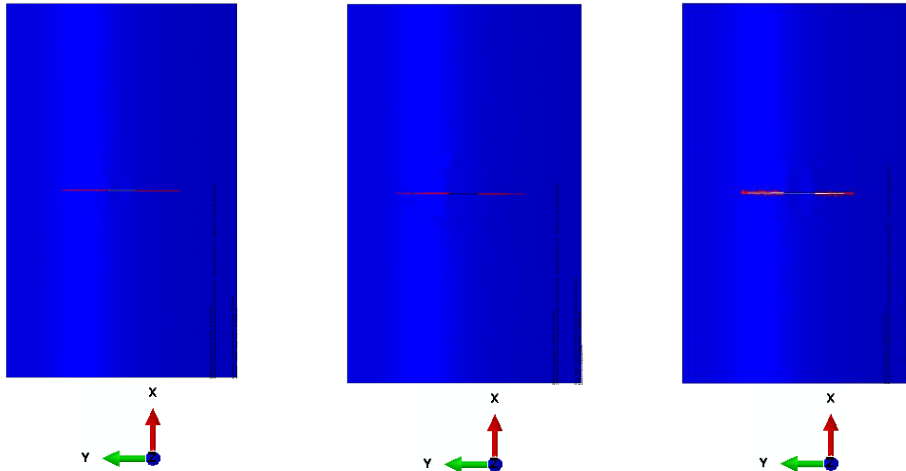
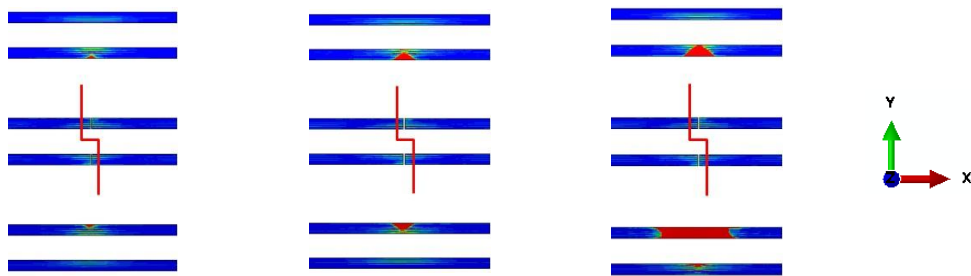


Figure 9. 7-stringer model tension load versus displacement responses.



a). TIED ABAQUS b). COH3D8 ABAQUS c). COH3D8 COSTR

Figure 10. 7-stringer model tension loading crack path predictions.



a). 91.6 kips load b). 96.7 kips load c). 109.4 kips load

Figure 11. 7-stringer COSTR model tension delamination progression.

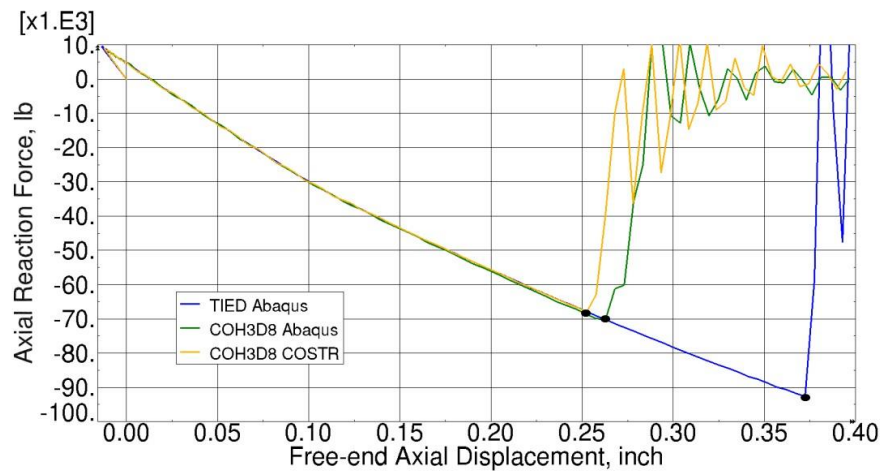


Figure 12. 7-stringer model compression load versus displacement responses.

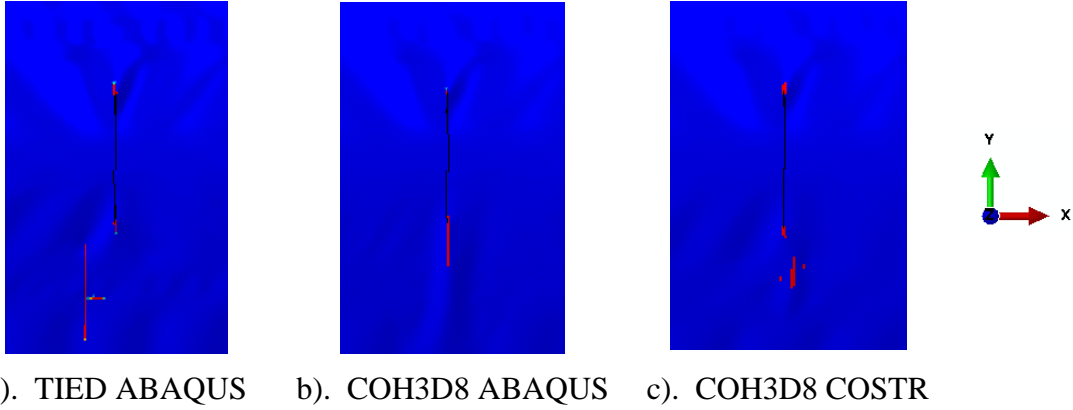


Figure 13: 7-stringer model compression loading crack path predictions.

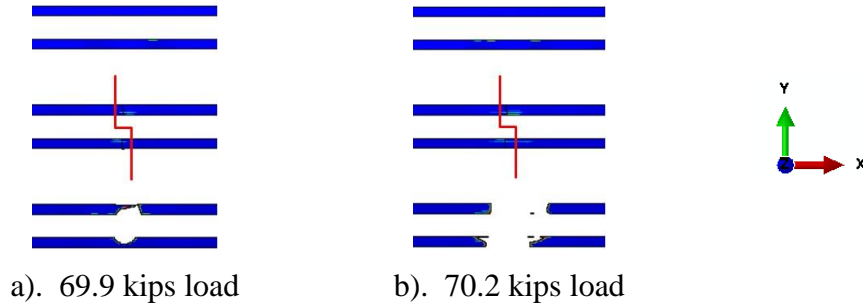


Figure 14. 7-stringer COH3D8 ABAQUS model compression delamination predictions.

For the compression loading case, the COH3D8 ABAQUS model predicts that delamination initiates at a reaction load of 60.2 kips. At this load level, the delamination cannot be seen in the COH3D8 element stiffness degradation contours. The delamination corresponding to reaction loads of 69.9 kips (failure onset) and 70.2 kips (failure) shown in Figures 14(a) and 14(b), respectively, can be seen in the COH3D8 ABAQUS model stiffness degradation contours, with more degradation at the adjacent intact stiffener.

IDEALIZED FUSELAGE PDA PREDICTIONS

The barrel has cantilever support conditions, consistent with anticipated future testing in NASA LaRC Combined Loads Test System (COLTS) Facility [7,8]. The loading is applied in two steps; the barrel is pressurized to 8.0 psi internal pressure in step one, and then with the pressure held constant, a rotation is applied at the free-end of the barrel in step two. This loading is intended to generically produce the response of an aircraft fuselage when performing a 2.5-g pull-up maneuver. The predicted response of the barrel down-bending case shown in Figure 15, depicted by adjacent illustration, using three different load rates is presented. The

predicted barrel failure loads corresponding to load rates of 0.210 rad/sec, 0.378 rad/sec, and 0.524 rad/sec are 10.95×10^6 in-lb, 8.92×10^6 in-lb, and 11.29×10^6 in-lb, respectively.

Unlike the 7-stringer model uniaxial tension and compression analysis cases, the barrel model is sensitive to load rate. In analyzing the barrel as described in the previous paragraph, either the top or bottom side is compressed, which tends to complicate the whole model response. To determine a load rate below which the change in failure prediction of the barrel is negligible, other analysis procedures have to be considered. For now, the load rate yielding the lowest failure load of the three analyses will be used in barrel predictions which are presented from this point forward. The barrel model predictions are presented in Figures 16 and 17, for the down-bending (crown tension) and up-bending (crown compression) cases, respectively.

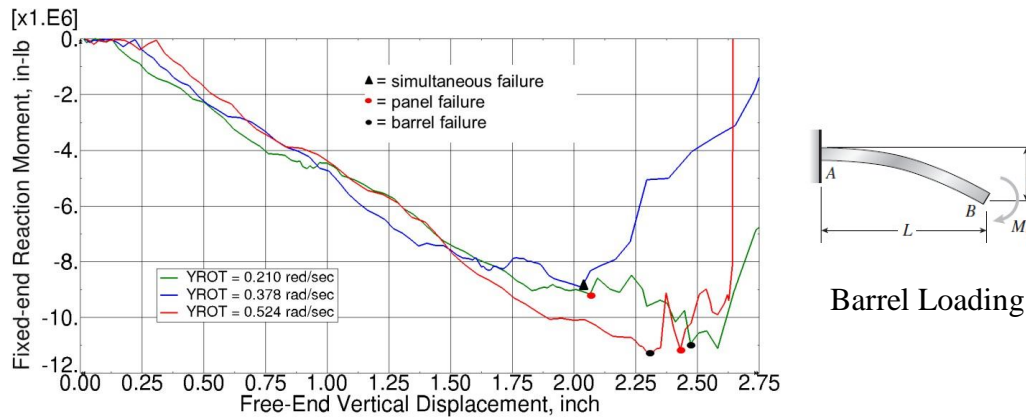


Figure 15. Load rate impact on Barrel TIED model down-bending analysis.

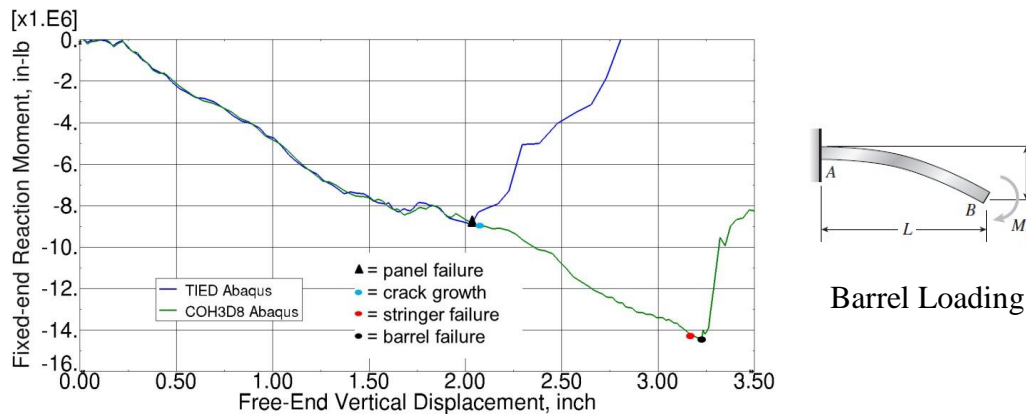


Figure 16. Barrel model down-bending analysis correlation.

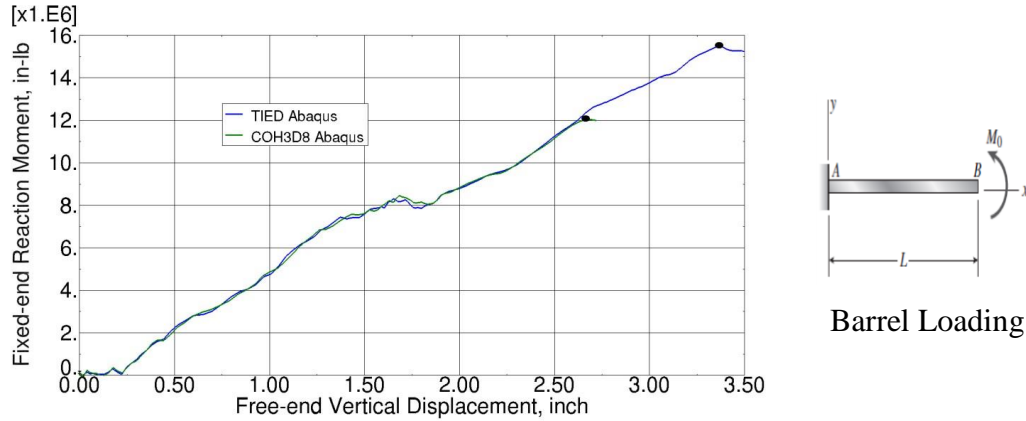
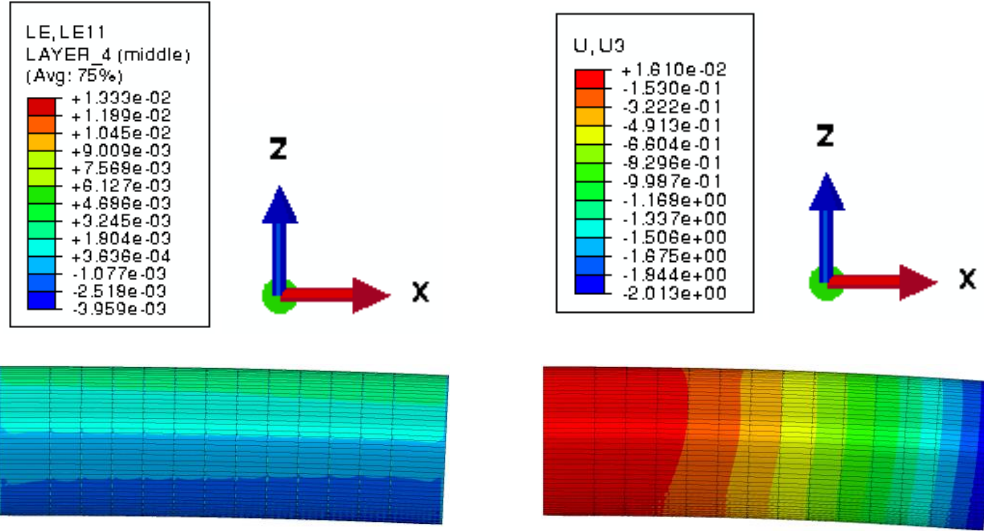


Figure 17. Barrel model up-bending analysis correlation.

The failure of the TIED model, shown with the crown in tension in Figure 16, is essentially a single event. However, the COH3D8 model continues to carry load, after having sustained extensive self-similar crack growth. The rationale for the COH3D8 model yielding a higher failure prediction is two-fold: (1) load redistribution takes place after events of crack growth and delamination [5], which decouples the skin and stringers in the central region of the panel surrounding the notch; and (2) the larger mesh size at the boundary of the refined mesh artificially impedes the progression of crack growth.

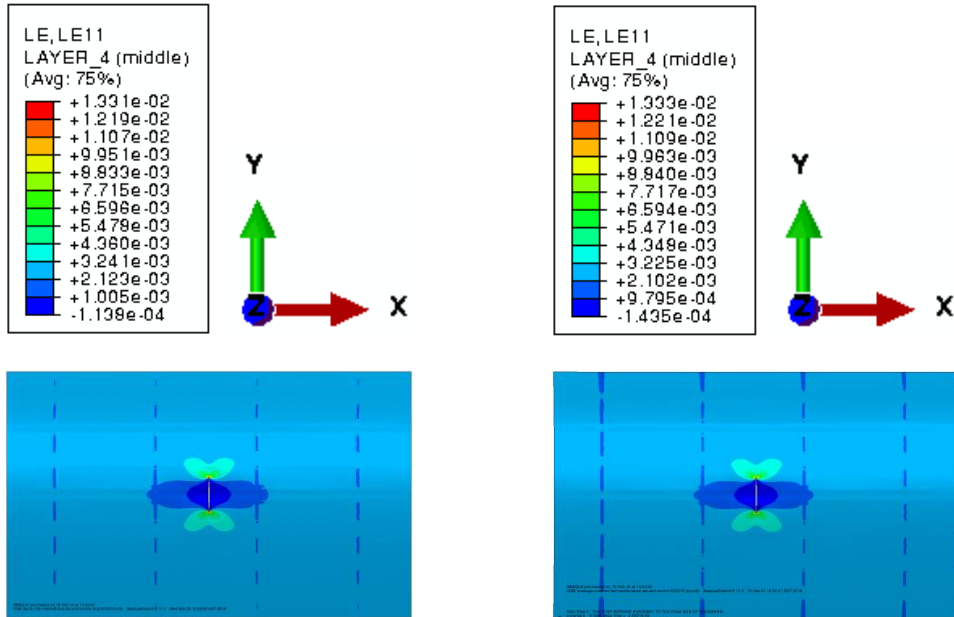
The barrel response presented in Figure 17 depicts that the barrel TIED model will carry a higher load in the up-bending load case than in the down-bending case. The TIED panel carries a higher load in compression because surprisingly buckling does not occur until the onset of failure. The barrel analysis longitudinal strain and vertical global deformation contours, respectively, are captured in Figures 18(a) and 18(b). The vertical deflection of the barrel just prior to panel failure is 1.97 inches. The analytical vertical deflection predictions at the free-end of the barrel have been closely approximated using beam formulas for a cantilever supported beam with applied end rotation. The strain contour plots of a zero degree ply (layer 4) of each model and their respective contour legends are presented in Figures 19(a) and 19(b). There is high degree of agreement of the values shown in the legends and the strain contours for a notched crown in tension.



a). Barrel global E11 strain

b). Barrel global U3 displacement

Figure 18. Barrel TIED down-bending analysis global response at onset of failure.



a). 7-stringer TIED model ply-4 strain

b). Barrel TIED model ply-4 strain

Figure 19. Barrel and 7-stringer panel down-bending analysis strain correlation.

CORRELATION OF 7-STRINGER AND BARREL PDA PREDICTIONS

The 7-stringer TIED model predictions shown in Figure 20 are correlated with the equivalent panel integrated into the barrel. The panel response produced by the barrel is captured by the discrete dots. The barrel panel internal force response was extracted from a free-body cut of the panel at mid-span using ABAQUS/viewer tools. The failure load obtained from the free-body of the panel at the mid-section was approximately 77.9 kips. This value correlates fairly well with the failure load obtained from the isolated 7-stringer panel analysis of 82.7 kips. The displacements obtained for the barrel panel were obtained directly from the predicted axial displacements of the centerline nodes at the forward and aft ends of the panel. The predicted crack paths for each model are depicted in Figures 21(a) and 21(b), and both models produced self-similar crack growth.

The 7-stringer model predictions are similarly correlated with the barrel predictions in Figures 22, 23, and 24. Again, the 7-stringer model predictions correlate well.

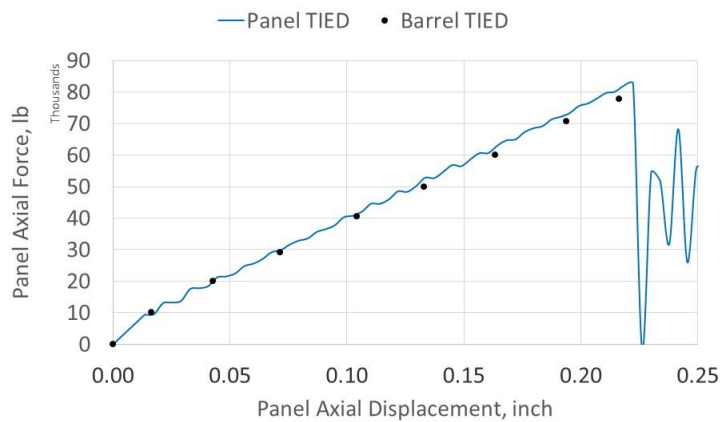
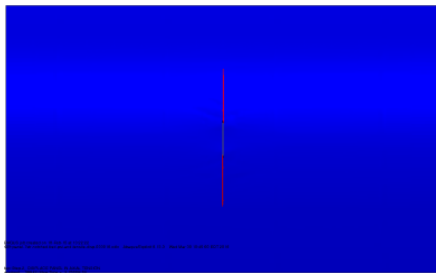
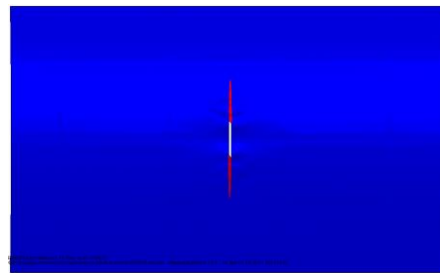


Figure 20. Barrel down-bending versus 7-stringer model tension correlation.



a). 7-stringer TIED model



b). Barrel TIED model

Figure 21. Barrel versus 7-stringer panel predicted crack paths.

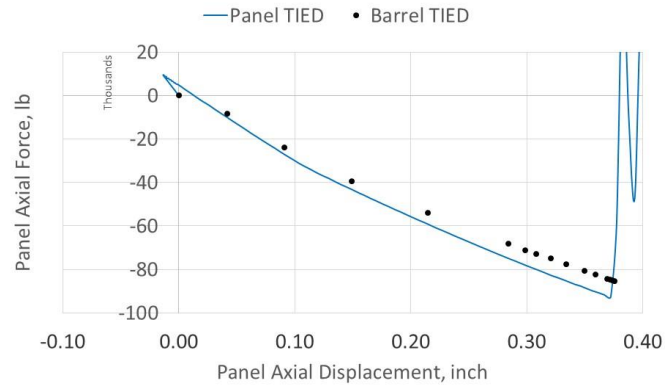


Figure 22. Barrel up-bending versus 7-stringer model compression correlation.

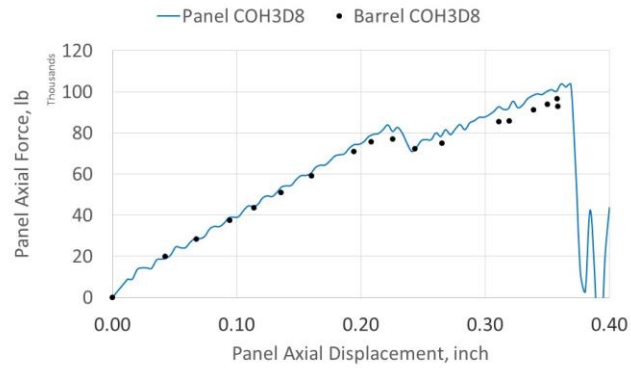


Figure 23. Barrel down-bending versus 7-stringer model tension correlation.

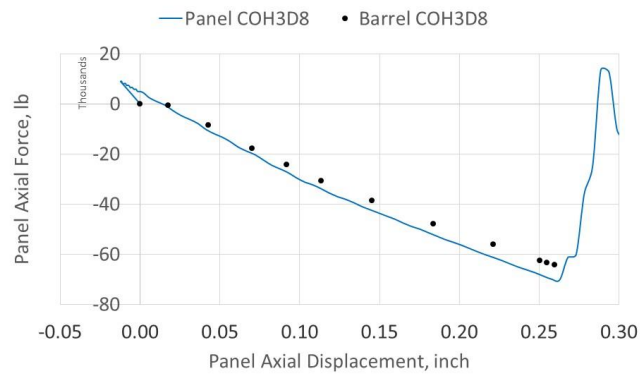


Figure 24. Barrel up-bending versus 7-stringer model compression correlation.

The barrel COH3D8 model up-bending longitudinal strain and vertical global deformation contours, respectively, are presented in Figures 25(a) and 25(b). The vertical deflection of the barrel just prior to failure is 2.48 inches. The strain contour plots of a zero degree ply (layer 4) of each model and their respective contour legends for the compression case are presented in Figures 26(a) and 26(b).

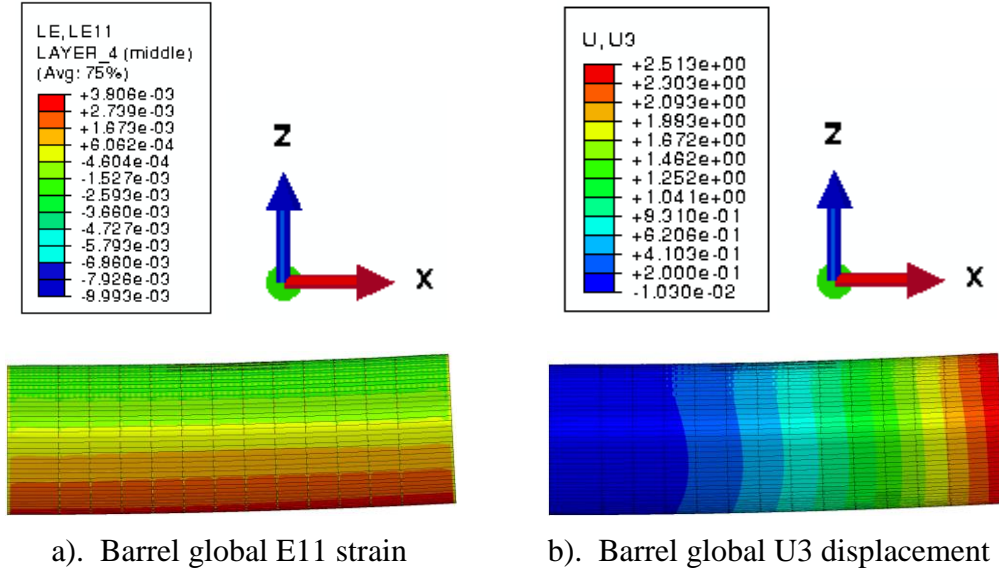


Figure 25. Barrel COH3D8 up-bending analysis global response at onset of failure.

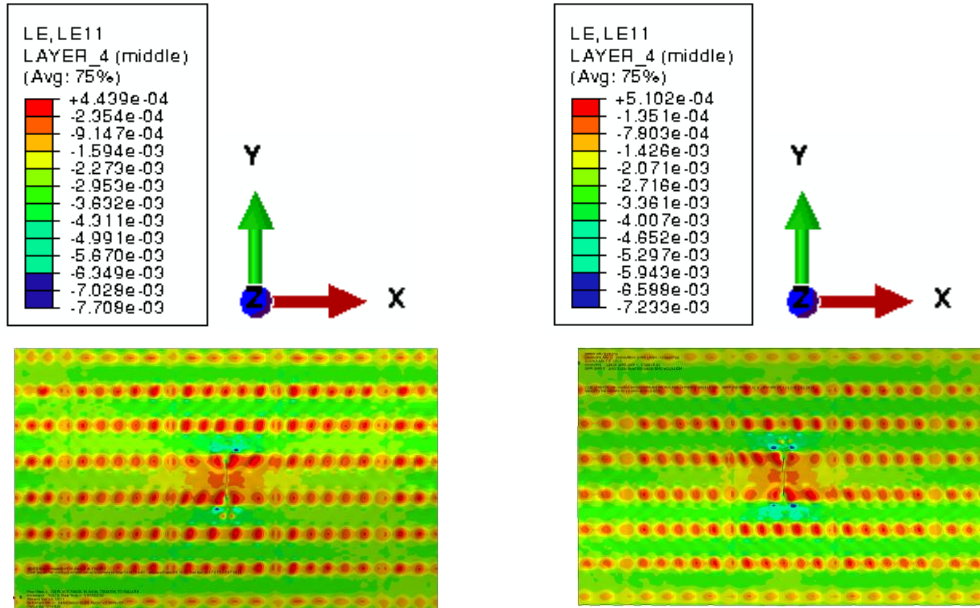


Figure 26. Barrel and 7-stringer COH3D8 up-bending analysis strain correlation.

The agreement of the values in the legends and the strain contours themselves is reasonably close.

CONCLUSIONS

The progressive damage analysis (PDA) of medium to large-scale models has been demonstrated using the ABAQUS/Explicit code. The capabilities of the built-in ABAQUS Hashin damage model and the COSTR damage model have been presented in the form of analysis predictions, which correlate responses of a curved composite 7-stringer panel against an idealized 8-ft diameter fuselage model. The particular TIED interface analysis predictions presented show that responses to tension and compression loading at the 7-stringer panel sub-component and vehicle levels are in general similar. Predictions for the COH3D8 model show that responses to tension and compression loading at the 7-stringer panel sub-component and vehicle levels are also in general similar. However, notch tip stresses can vary substantially. Though failure load predictions are generally within 10%, the response correlations of curved panels of varying scale, which contain large 2-bay longitudinal cracks, may reflect a higher degree of disagreement. The COH3D8 ABAQUS damage model captured the possibility of load redistribution occurring on both scales.

Results presented in this paper indicate that the load rate impacts the barrel structure predictions. Applying an end-moment or rotation to the free-end of the cantilever fuselage structure produces tension and compression reactions concurrently, the combined response of which varies based on the input. The slowest load rate tends to capture the proper sequence of events, but ironically does not yield the lowest failure load prediction.

Regarding the sub-component scale, it is important to note that load redistribution may not be captured or accounted for when analyzing and/or testing smaller sub-components. In the 3-stringer model predictions shown, the initial load drop and final failure, respectively, for all three models are one in the same event. However, for the 7-stringer model, load redistribution is predicted, particularly for the COH3D8 ABAQUS model case. The difference between the loads at which initial failure and final failure occurs is approximately twenty percent: a substantial difference to consider when reporting the load carrying capacity of a specimen.

The intent of this numerical study was to address potential issues associated with modeling and analyzing large curved structures subjected to flight maneuver loadings. The next step is to validate the modeling techniques discussed herein with test data from relevant experiments sponsored by NASA Advanced Composites Program and other industry sources.

REFERENCES

1. Mohaghegh, M. 2005. "Validation and Certification of Aircraft Structures," Proceedings of the 46th AIAA/ASME/ASCE/AHS/ASC Structures, Structural Dynamics and Materials

- Conference, AIAA paper No. AIAA-2005-2162, Engineering Technology Development Boeing Commercial Airplanes.
2. © Dassault Systemes, 2013. "Damage and Failure for Fiber Reinforced Composites: Overview," in *ABAQUS Analysis User's Guide*, Version 6.13, Section 24.3.1.
 3. Satyanarayana, A., Bogert, P., Karayev, Z. K., Nordman, S. P., Hamid, R. 2012. "Influence of Finite Element Size in Residual Strength Prediction of Composite Structures," Proceedings of the 53rd AIAA/ASME/ASCE/AHS/ASC Structures, Structural Dynamics and Materials Conference, AIAA paper No. AIAA-2012-1619, Analytical Mechanics Associates, Inc. resident at NASA Langley Research Center Structural Mechanics and Concepts Branch, Hampton, VA.
 4. Bogert, P., Satyanarayana, A., Chunchu, P. 2006. "Comparison of Damage Path Predictions for Composite Laminates by Explicit and Standard Finite Element Analysis Tools," Proceedings of the 47th AIAA/ASME/ASCE/AHS/ASC Structures, Structural Dynamics and Materials Conference, AIAA paper No. AIAA-2006-1750, NASA Langley Research Center Structural Mechanics and Concepts Branch, Hampton, VA.
 5. Satyanarayana, A., Bogert, B. P., Chunchu, B. P. 2007. "The Effect of Delamination on Damage Path and Failure Load Prediction for Notched Composite Laminates," Proceedings of the 48th AIAA/ASME/ASCE/AHS/ASC Structures, Structural Dynamics and Materials Conference, AIAA paper No. AIAA-2007-1993, Analytical Services & Materials, Inc. resident at NASA Langley Research Center Structural Mechanics and Concepts Branch, Hampton, VA.
 6. Turon, A., Davila, C. G., Camanho, P. P., Costa, J. 2007. "An Engineering Solution for Mesh Size Effects in the Simulation of Delamination Using Cohesive Zone Models," *Engineering Fracture Mechanics*, vol. 74, 1665–1682, 2007.
 7. Rouse, M. 2013. "Methodologies for Combined Loads Test Using a Multi-Actuator Test Machine," Proceedings of the SEM Annual Conference and Exposition on Experimental and Applied Mechanics, paper No. 20130014926, NASA Langley Research Center Structural Mechanics and Concepts Branch, Hampton, VA.
 8. Gould, K. Satyanarayana, A., Bogert, P. December 2010. "High Speed Research Fuselage Composite Crown Panel 67 Test Report," Analytical Services & Materials, Inc. resident at NASA Langley Research Center Structural Mechanics and Concepts Branch, Hampton, VA.